CrossMark

TECHNICAL PAPER

An effective structural health monitoring methodology for damage isolation based on multisensor arrangements

Pablo Rodrigo Souza[1] · **Eurípedes Guilherme Oliveira Nóbrega**[2]

Abstract The development of strategies to evaluate health of mechanical structures has been studied by the international community due to their potential application in the prevention of failures and optimization of maintenance procedures. These systems requires digital signal processing algorithms and interpretation methods, which aim to extract parameters sensitive to the rise of discontinuities in the material from measurements, to classify signal events to detect the damage onset. This paper proposes a simple and effective methodology for monitoring the integrity of mechanical structures, based on Lamb wave and pitch–catch approach, through analysis of signals generated by multisensor arrangements. These signals are processed by discrete wavelet and Hilbert transform, intended to improve peak amplitude estimation, through noise and dispersion reduction. Assessment of structure's integrity proceeds through the joint analysis of damage indices calculated from the discrepancy of the maximum amplitude of the signal measured by each sensor of the arrangement. Experimental application of the method to an aluminum plate showed its effectiveness to detect, localize and evaluate damage severity in established regions of the monitored area, including the case of two simultaneous damages.

1 Introduction

The assessment of structural condition is typically an inverse problem in which parameters extracted from measured signals are used to detect and isolate damages. In most cases, the use of a single sensor is not able to provide sufficient information to structural interrogation because of uncertainty, imprecision and lack of complementary data [1]. To improve the monitoring system robustness, multisensor arrays should be applied in which each sensor provides parameters to assess the integrity of the region where it has greater sensitivity, leading to precise and clear estimate of damage characteristics, such as its location, shape, severity and others. Moreover, the combination of these parameters guarantees consistency among data obtained from different sensors of the arrangement. There are several application examples of multisensor arrangements for monitoring the integrity of structures. Zhao et al. [2] compared some tomographic imaging techniques to image reconstruction of an aluminum plate from parameters extracted of signals corresponding to the Lamb waves propagation. Three types of arrangements were evaluated: circular, squared and parallel lines. One problem with the use of these techniques is the large number of signals that need to be processed to obtain the image. Using sixteen transducers, the circular arrangement has 240 signals, the squared 192 and the arrangement formed by two parallel lines 128. The time needed for image reconstruction can become unfeasible for real time applications. Giridhara et al. [3] proposed a methodology based on a circular array of piezoelectric transducers to localize and evaluate the severity

Technical Editor: Marcelo A. Savi.

✉ Pablo Rodrigo Souza
  pablo@ifsp.edu.br

  Eurípedes Guilherme Oliveira Nóbrega
  egon@fem.unicamp.br

1 Federal Institute of São Paulo, Piracicaba, São Paulo, Brazil

2 Faculty of Mechanical Engineering, University of Campinas, Campinas, São Paulo, Brazil

1352

J Braz. Soc. Mech. Sci. Eng. (2017) 39:1351–1363

of corrosion in metallic plates. The symmetry breaking of signals pattern measured by three adjacent sensors indicate damage on the structure. Then, parameters extracted from these signals are used in a triangulation scheme to localize and evaluate damage severity. However, nonidentical bonding of these sensors to the plate can break the symmetry even for an undamaged structure [4]. Su et al. [5] developed a sensor network formed by a set of miniaturized piezoelectric wafers connected by a thin and flexible printed circuit board to monitor the integrity of composite structures using Lamb waves. This sensor network has been embedded into composite laminate during the manufacturing process. Merging data from signals measured from multiple paths led to detection and location of delamination. Malinowski et al. [6] used a triangular arrangement with four piezoelectric transducers at each vertex to detect and locate damage inside, outside and between two vertices of the triangular region. The numerical algorithm proposed in this paper uses the group velocity of the wave packet and the time of flight between the actuator and the damage, and between the damage and the sensor to determine its location. This can result in errors due to mode conversion when the incident wave interacts with damaged region, because in this case there is also a change in the group velocity of this new mode.

The study of new multisensor arrays and the definition of strategies to merge the parameters extracted from signals to detect, locate and assess the severity of damage is a significant contribution to the development of structural health monitoring systems. This paper proposes a method for monitoring the integrity of mechanical structures based on the propagation of Lamb waves and on the fusion of parameters extracted from the signals processed by discrete wavelet transforms (DWT) and Hilbert transform (HT). A circular arrangement with a centered actuator was used to enable damage isolation in different regions inside a monitored area of an aluminum plate. The ability to isolate more than one region damaged simultaneously was also evaluated. The discrepancy of the maximum amplitude of the signal measured by a sensor was adopted as damage index.

2 Lamb waves and signal processing techniques

One of the most used approaches to assess the structural integrity is through Lamb waves propagation [7–9]. These waves can be generated and measured using piezoelectric transducers. The information about the presence of damage, its location and severity can be obtained by analyzing the parameters of the reflected and transmitted waves resulting from the interaction between the incident wave and the damage. There are basically two methods for using Lamb waves known as pitch–catch and pulse-echo [10].
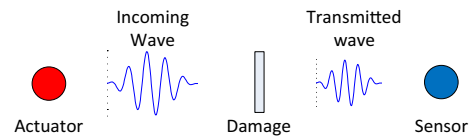

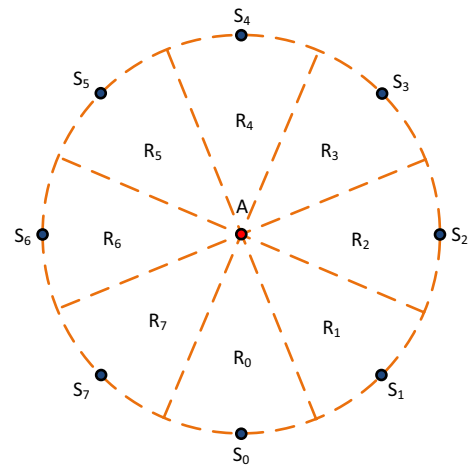**Fig. 1** Positioning of transducers to the pitch–catch approach

Fig. 2 Circular array of piezoelectric transducers and its respective monitored regions

The simplest pitch–catch approach relies on the signal parameter changes, extracted from the transducers' Lamb wave transmission, as illustrated in Fig. 1. It is seen in this figure an actuator emitting a burst signal, which is captured by a sensor, both piezoelectric patch. This signal incorporates the medium characteristics between the transducers. Damage onset on this region causes scattering of the waves, which modifies some measured signal parameters. Comparison between a known signature of the healthy structure and an actual measured signal may conduct to damage detection and identification. Change of parameters may occur also if the damage is not in the direct line between the transducers.

Using multisensor array allows to precisely localize damage position, and improves confidence in its diagnosing. Figure 2 shows a circular array formed by eight sensors (S_0–S_7) and an actuator (A). Each sensor monitors a region (R_x) corresponding to one-eighth of the total area. This arrangement can be used to monitor critical areas of the structure that are more subject to damage occurrence and can compromise its integrity, for example, the MD Explorer helicopter flexbeam [11], or for monitoring the effectiveness of structural repairs applied over damaged areas.

Signals from the measuring system need to be processed by specific algorithms to separate information from noise, regular reflections and other interferences in the system.
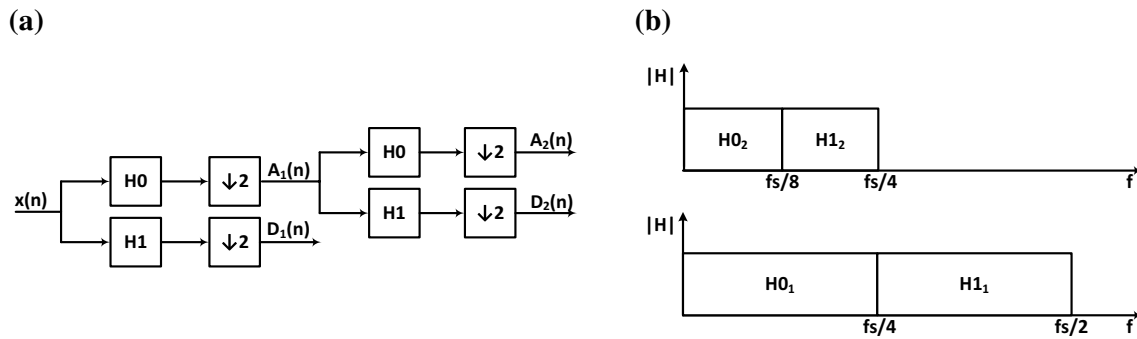
Fig. 3 Filter bank for DWT: **a** two level analysis and **b** frequency range of high and low pass filters

The wavelet transform is a signal processing technique used to represent signal features in time and frequency domains simultaneously. It has the ability to detect aperiodic short-time events, unlike the Fourier transform which is particularly useful for the analysis of periodic signals. These transient events are detected through the similarity between its shape in time domain and a waveform known as mother wavelet. The continuous wavelet transform (CWT) of a signal $x(t)$ is given by:

$$\gamma(s, \tau) = \int x(t)\Psi_{s,\tau}^{*}(t)\mathrm{d}t \tag{1}$$

where * denotes complex conjugate, s the frequency scale and τ the translation in time. Equation (1) represents the projection of $x(t)$ on an orthonormal base of functions, dilated by s and translated by τ, generated by a function called mother wavelet given by:

$$\Psi_{s,\tau}(t) = \frac{1}{\sqrt{2}}\Psi\left(\frac{t - \tau}{s}\right) \tag{2}$$

This approach fits well to analyze nonstationary signals, because its spectral components vary along time. The propagation of Lamb waves is an example of signal with punctual occurrences. Mallat [12] presented an efficient method to implement the wavelet transform in discrete time, through multiresolution analysis and digital filter banks. This theory relates the DWT with a filter bank composed by high and low pass quadrature mirrored filters, through which the signal is decomposed into details and approximations. The approximation is obtained as the output of the low pass filter and is related to the smoothed signal. The output of the high pass filter provides the details of the signal, related to transient events contained in the signal. Figure 3a shows the layout of the filter bank, composed by high pass filter (H1) and low pass filter (H0), for two levels of resolution. The symbol ↓2 represents down-sampling or decimation of the filtered signal. Each decomposition level separates the spectral components at frequency bands, which depends of the sampling frequency (fs) of the signal acquired. Figure 3b

shows the frequency response of high and low pass ideal filters for two level decomposition DWT.

Higher frequency signal components are located at lower level details. Analyzing the signal decomposed into several details provides information that could be hidden in the original signal, probably masked by noise from the measurement system. The subdivision of the signal spectrum in several frequency bands, through the filtering process, is equivalent to the scaling s of (2). On the other hand, the translation τ of this equation is obtained by convolution of the signal with the filter coefficients. One significant advantage of using the DWT approach for signal processing is to design high and low pass filters as digital filters on programmable logic devices, such as modern FPGAs. This enables the algorithms implementation directly in hardware, which leads to the high performance needed in real time signal processing applications [13–15] and ultimately to embedded monitoring systems.

The Hilbert transform can be used to create an analytical signal from a real signal [16]. Consider $x(t)$ a real signal. The analytic signal $x_{\mathrm{a}}(t)$ is calculated as follows:

$$x_{\mathrm{a}}(t) = x(t) + iH\{x(t)\} \tag{3}$$

where $H\{x(t)\}$ is the HT of the real signal. An effective approach to calculate the HT is as follows:

1. Calculate the Fourier Transform of the signal
2. Rotate the phase of the signal obtained at 90°
3. Return to time domain calculating the inverse Fourier transform.

Writing the analytical signal in polar form, we have:

$$x_{\mathrm{a}}(t) = Ae^{-j\varphi} \tag{4}$$

where A is the absolute value and φ is the phase of the analytical signal. The absolute value of the analytical signal corresponds to signal envelope.

To illustrate the effect of applying these techniques on measured signals by piezoresistive sensors, Fig. 4 shows
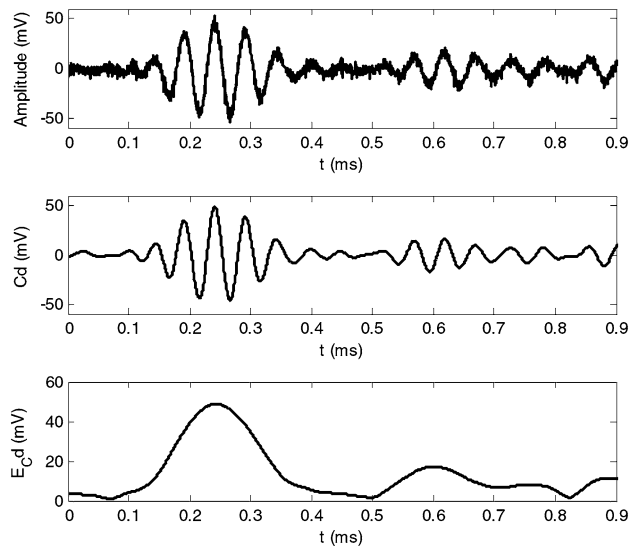
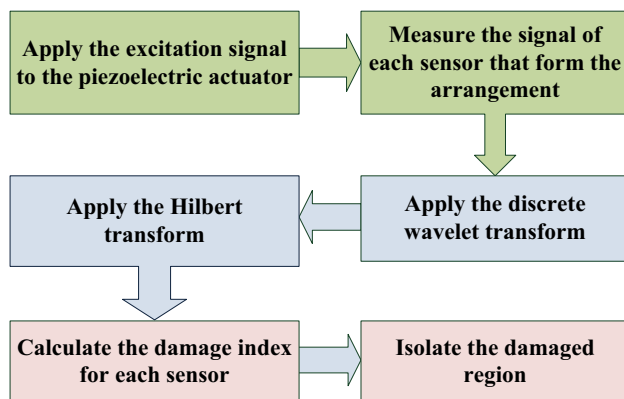**Fig. 4** Signal measured by sensor S_7, detail coefficients of DWT and its envelope

Fig. 5 Method for monitoring the integrity of an area using a circular array of piezoelectric transducers

the signal measured by S_7, the detail coefficients of sixth level of its DWT with the mother wavelet Daubechies 40 and its envelope. It clearly minimizes the noise present in the measurement system enhancing the signal desired attributes. The peak amplitude and the instant they occur are much more evident on the signal envelope. These parameters can be used to monitoring the integrity of the structure.

3 Method description

Figure 5 shows a block diagram that represents the method for monitoring the integrity of structures, using the circular array of piezo transducers shown in Fig. 2.

The procedure begins with generation of the excitation signal by the central actuator and its measurement by one of the sensors arrangement. These steps are repeated for all sensors of the circular array. DWT and HT are applied to get the envelope of DWT's detail coefficients to emphasize the magnitude and position of the first peak of the processed signal. Detection, localization of the damaged region and also assessment of damage severity result from the joint analysis of the damage indices (DI), calculated from the envelope data for each sensor of the array. This index is defined by the percentage difference between the peak amplitudes of the processed signals obtained from healthy structure (A_h) and the damaged structure (A_d), given by:

$$DI\% = \frac{A_h - A_d}{A_h} \times 100 \qquad (5)$$

According to (5), a decrease on the signal amplitude results in a positive DI. On the other hand, a negative DI indicates an increase on the signal amplitude.

4 Experimental procedure

The experiments were conducted on a rectangular aluminum plate of 70 cm × 50 cm × 1 mm to assess the method efficacy to detect, localize and evaluate the damage severity. The experimental setup shown in Fig. 6 consists of nine circular buzzers of 20 mm diameter forming a circular arrangement with a centered actuator with 10 cm radius. A tone burst containing five cycles of a 20 kHz sine wave, multiplied by a Hanning window, was applied to the central actuator using an Agilent 33120A arbitrary waveform generator. An analog multiplex, with an instrumentation amplifier per channel using the Analog Devices AD620, was developed, including an anti-aliasing filter using the universal active filter UAF42. An Agilent 54622A oscilloscope was used to acquire the signals with a sample frequency of 2 MHz, and to transmit the raw data to be processed and analyzed using MatLab®. Mother wavelet Daubechies 40 was adopted in the DWT for all signals and the detail coefficients of sixth level corresponds to the Lamb wave propagation.

In the validation of a nondestructive testing technique, it is necessary to induce artificial damages in the structure, such as cracks, corrosion, delamination and others to evaluate their effectiveness. These types of damages undertake permanently the structural integrity preventing its use for other tests, which can be impractical in tests with complex and high cost structures. In such cases, pseudo-damages can be used to enable the use of the same structure in a large variety of tests, since they do not cause permanent
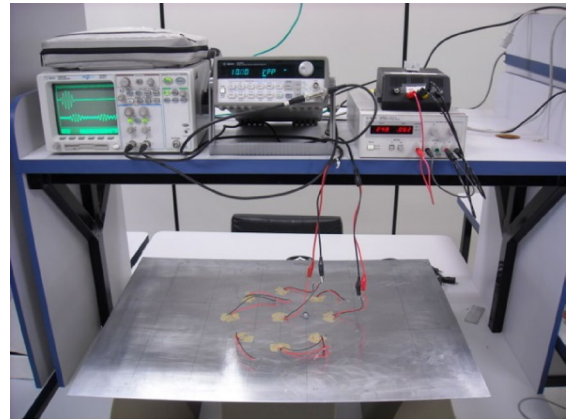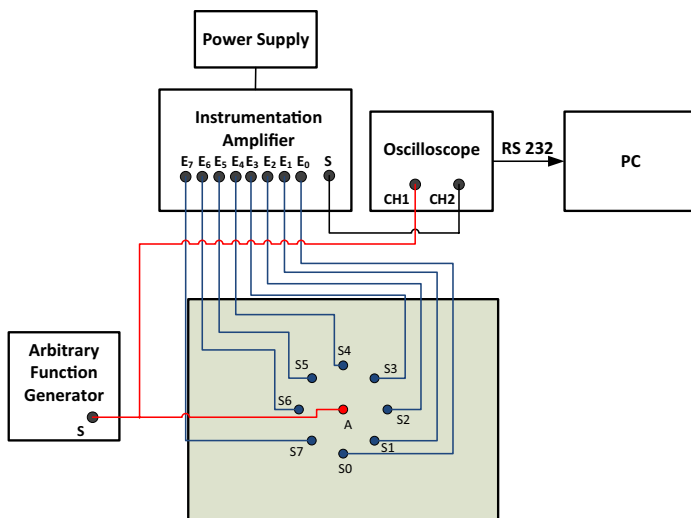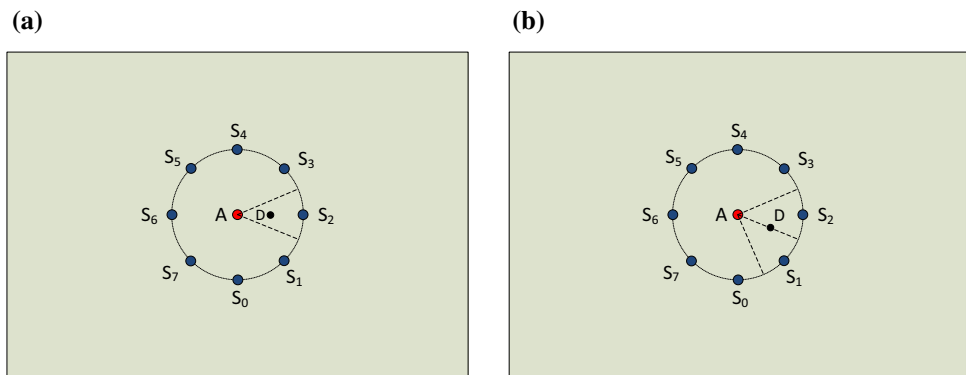
J Braz. Soc. Mech. Sci. Eng. (2017) 39:1351–1363

1355

Fig. 6 Experimental setup

Fig. 7 Damage (D) localized at: **a** region R_2 and **b** at the boundaries of regions R_1 and R_2

changes in the properties of the structure, such as stiffness, mass and acoustic impedance. Pfeiffer and Wevers [17] used two iron cubes pressed against each side of an aluminum plate and Kessler and Shim [18] used a rectangular weight to simulate the same effect, as a real damage would have on the propagation of Lamb waves.

In this work, a spherical mass of 30 g was used to obtain a punctual mass change on the plate, which may represent damage. This mass was placed in the middle of the line formed by the actuator and sensors S_2, S_4, S_6 and S_7 to demonstrate the ability to locate the damaged region inside the circular area, with each region tested separately. Measurements for the mass positioned among the actuator and the sensors S_1 and S_2 and among the actuator and the sensors S_4 and S_5 were made to verify the effectiveness of the proposed method to locate damage at the boundary of two regions. To illustrate these experiments, Fig. 7a shows the cases for the mass positioned at region R_2 and Fig. 7b for the mass positioned at the boundaries of regions R_1 and R_2.

Three different masses of 20, 40 and 60 g were positioned between the actuator and sensor S_2 to demonstrate the method's ability to assess damage severity.

To explore the possibility to reduce the area of the isolated region, increasing the resolution of the monitoring system, a two ring-shaped arrangement of piezo transducers with 20 and 40 cm radius were used to monitor the integrity of an aluminum plate with 1 m × 1 m × 1 m, as shown in Fig. 8. In this case, the monitored area was divided into sixteen regions, eight internal regions (Rx_i) and eight external (Rx_e) to ring formed by the Sx_i sensors.

Looking for a thorough test of the arrangement, the mass was first positioned in regions $R0_i$, $R3_i$, $R5_e$ and $R7_e$ to simulate damage. To complete the experiments, two masses were positioned simultaneously in regions $R1_i$ and $R6_e$ to indicate the behavior under two damages at the same time.

To compare results obtained with the proposed damage index (5), it was chosen the root mean square deviation (RMSD), a damage index widely used to assess structural integrity [19, 20]. RMSD is defined as:
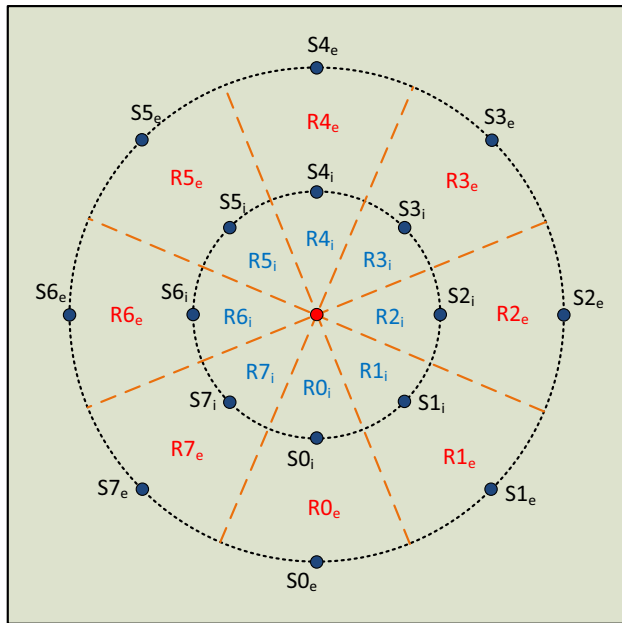
Fig. 8 Two ring-shaped arrangement of piezo transducers to monitor the area divided into 16 regions

Fig. 9 Variation of signals measured by sensors for healthy plate

$$\text{RMSD\%} = \sqrt{\frac{\sum_i^N (\text{Ed}_i - \text{Eh}_i)^2}{\sum_i^N (\text{Eh}_i)^2}} \times 100 \qquad (6)$$

where, Ed and Eh are the envelopes of signals for damaged and healthy structure, respectively. According to (6), the greater the index, the more severe the damage is.

5 Results and discussion

To evaluate changes in the first peak of signal envelope due to the uncertainties in measurement system, six samples from each sensor of the arrangement (Fig. 6) were measured from the healthy plate. For sensor S_i, the expanded uncertainty is given by:

$$u_i = 2.57 \times \sigma_i$$

where σ is the standard deviation and 2.57 is the coverage factor for a 95 % confidence level for the *t*-student distribution with five degrees of freedom [21]. Figure 9 shows values obtained for the eight sensors of the arrangement. Sensor S4 showed the greatest variation, corresponding to 0.26 %. Therefore, signal changes greater than this value indicate the onset of damage on the structure.

Figure 10 shows the signal envelope of the eight sensors with the 30 g mass positioned between the actuator and the sensor S_7. Clearly, signal measured by sensor S_7 suffered a significant reduction, while for the other sensors there was no expressive change. The DI for S_7 was 46.2 %. For
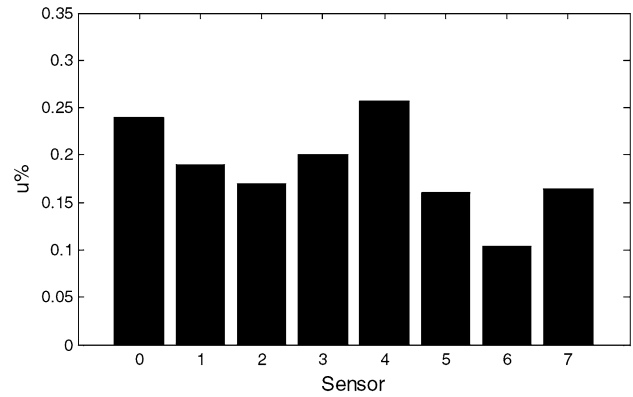
the other sensors, the highest DI was 5.6 % for S_2. Similar results were obtained for RMSD index, in which the greater value was 30.5 for S_7. The DI and RMSD of each sensor of the arrangement for the damage positioned in regions R_2, R_4, R_6 and R_7 are shown in Table 1. In all cases, the sensor positioned after the damage presented the greater DI and RMSD. Therefore, the highest damage index indicates damaged region.

For the mass positioned among the actuator and two sensors, there was no decrease in the first peak of signal envelope for sensors nearest of the damage. Instead, DI of these sensors presented negative values indicating an increase in the amplitude of the signals as may be seen in Fig. 11a for damage at the boundary of regions R_1 and R_2 and Fig. 11b for damage at the boundary of regions R_4 and R_5. This occurs due to part of the reflected wave in the damage adds to the incident wave resulting on an increase of the amplitude of the measured signal. Therefore, the two sensors that presented the most negative DI, isolate the damage at the boundary of regions monitored by them.

Results obtained with RMSD index were ambiguous. Although Fig. 11c shows that sensors S_1 and S_2 presented the highest values for RMSD with damage at the boundary of R_1 and R_2, the RMSD value for S_3 was also considerable, leaving doubt if damage location is at region R_2 or at the boundaries of R_1 and R_2 or R_2 and R_3. A similar analysis for damage at the boundary of regions R_4 and R_5 can be made from Fig. 11d.

Confirmed the method's effectiveness in detecting and isolating the damaged region, another experiment was made to verify the DI ability to evaluate damage severity. Figure 12 shows the envelope of DWT coefficients of signals measured by S_2 for the healthy plate, and with three masses of 20, 40 and 60 g positioned between actuator and this sensor to simulate the increase of damage severity. As expected, the increase in mass resulted in a reduction of the amplitude of the first peak of the signal measured by
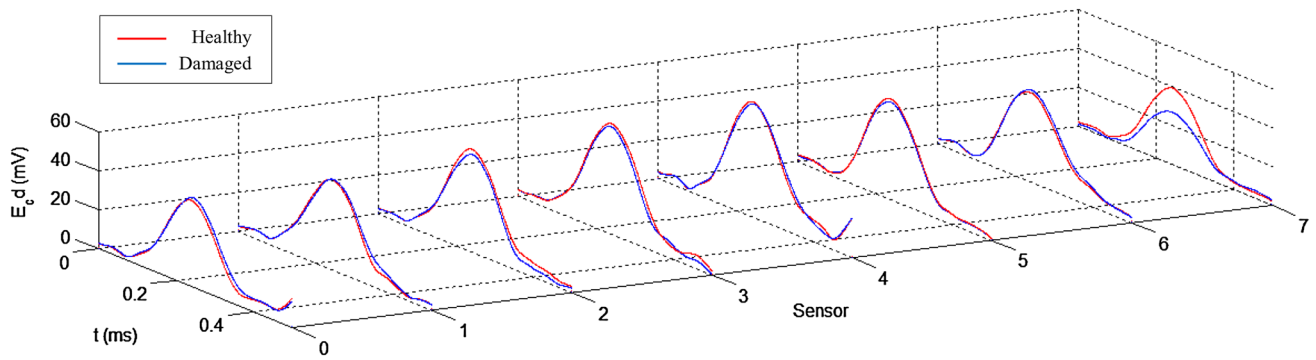
Fig. 10 Envelope of DWT coefficients of signals measured by sensors for damage at R_7

Table 1 Damage indices DI and RMSD for regions R_2, R_4, R_6 and R_7 damaged

		S_0	S_1	S_2	S_3	S_4	S_5	S_6	S_7
R_2	DI	0.2	9.5	**25.6**	5.2	5.9	1.0	7.6	4.5
	RMSD	6.7	9.2	**26.4**	5.2	10.3	6.0	16.4	14.0
R_4	DI	0.9	4.6	11.3	10.1	**39.9**	19.7	7.5	3.8
	RMSD	6.9	6.6	16.5	10.8	**39.1**	20.5	11.8	5.7
R_6	DI	4.0	1.4	5.0	2.6	11.9	3.5	**25.9**	2.1
	RMSD	5.9	9.3	6.7	6.9	15.9	5.1	**37.9**	6.2
R_7	DI	3.8	0.6	5.6	3.0	1.7	3.3	3.1	**46.2**
	RMSD	8.3	7.0	8.6	7.2	4.8	3.5	5.8	**30.5**

Bold values highlight the highest damage indices
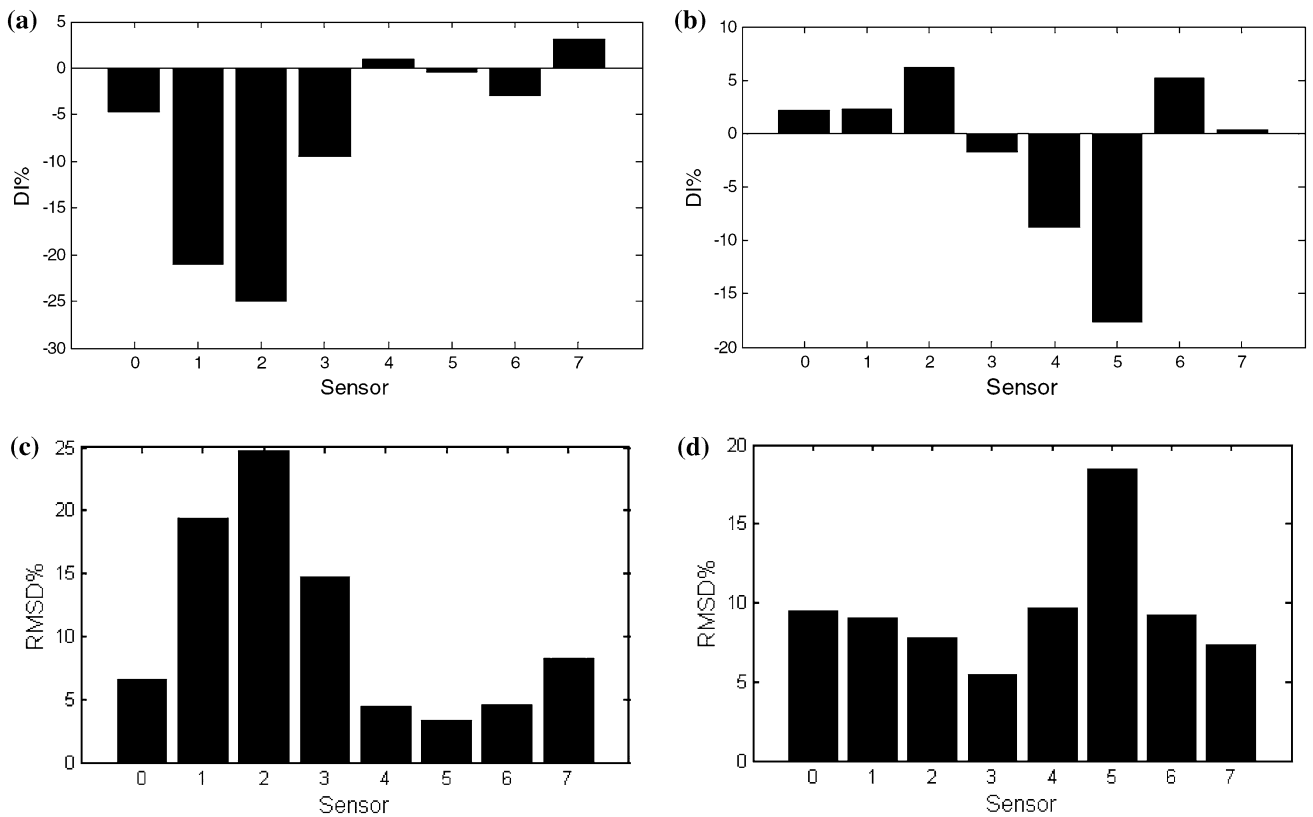
Fig. 11 Damage indices: **a**, **b** DI and **c**, **d** RMSD for damage at boundary of two regions

1358

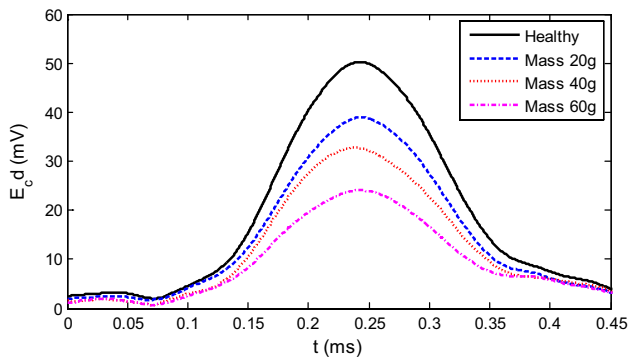J Braz. Soc. Mech. Sci. Eng. (2017) 39:1351–1363

Fig. 12 Envelope of DWT coefficients of signals measured by S_2 for healthy plate and with three masses positioned at region R_2

S_2. Table 2 shows the DI and RMSD for the eight sensors of the arrangement. In the three cases, the highest DI was calculated for the sensor S_2 and it increased monotonically as the value of the mass increased, indicating the damage severity degree. For the other seven sensors, the DI was lower, making it clear that region R_2 is damage. The values of RMSD were quite close to DI for S_2, indicating that both indices were effective to evaluate the damage's severity with the same level of sensitivity.

For the first experiment with the two ring-shaped arrangement, considering damage positioned on internal region $R0_i$ (Fig. 8), signal amplitude was reduced significantly only for $S0_i$ and $S0_e$. The envelope of DWT

Table 2 Damage indices DI and RMSD of damage severity experiment

		S_0	S_1	S_2	S_3	S_4	S_5	S_6	S_7
Mass 20 g	DI	4.6	13.0	**22.5**	17.8	2.1	2.3	0.6	3.1
	RMSD	7.3	14.6	**22.7**	17.5	3.9	7.9	9.4	6.9
Mass 40 g	DI	3.6	0.6	**34.8**	0.6	2.8	0.9	2.11	5.3
	RMSD	5.0	2.8	**34.3**	4.5	3.9	3.8	15.5	15.3
Mass 60 g	DI	7.7	1.5	**52.1**	0.7	7.1	1.3	6.2	3.6
	RMSD	11.7	8.0	**51.4**	3.5	9.6	14.7	13.9	8.7

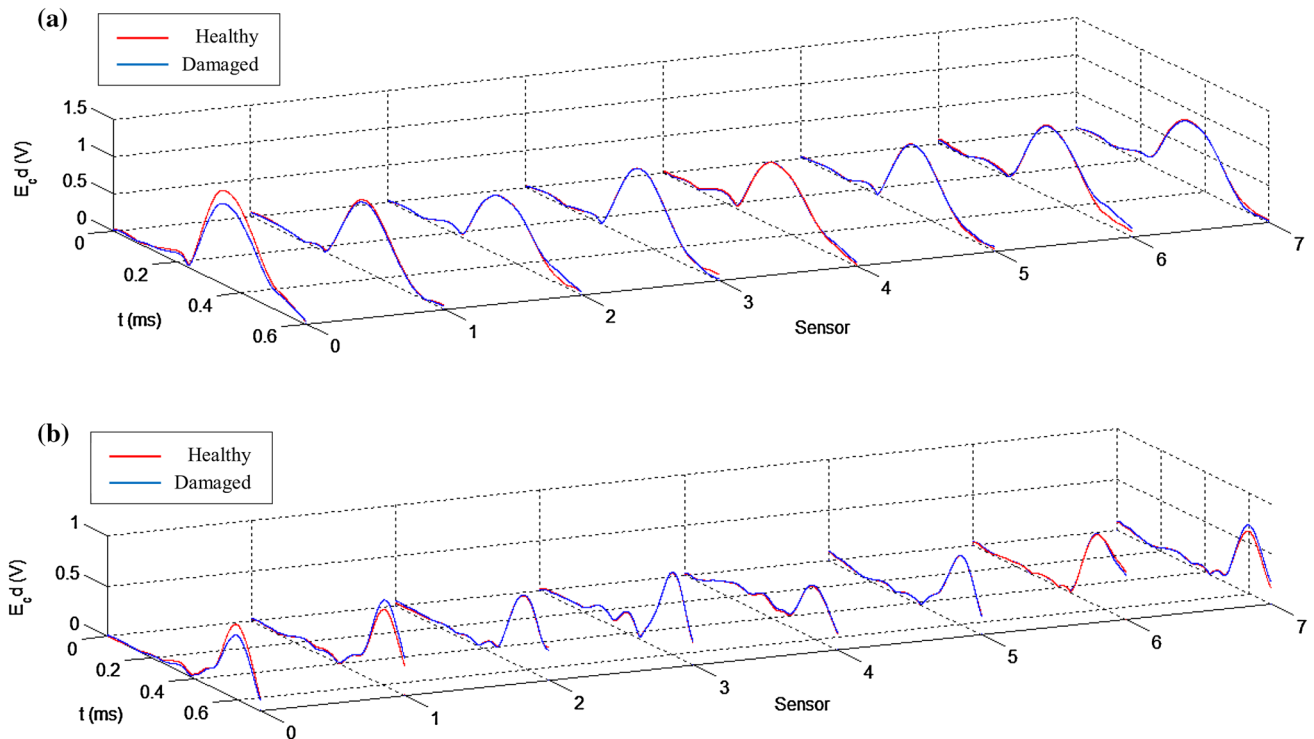Bold values highlight the highest damage indices

Fig. 13 Envelope of DWT coefficients of signals measured by sensors of: **a** internal and **b** external ring for damage at $R0_i$
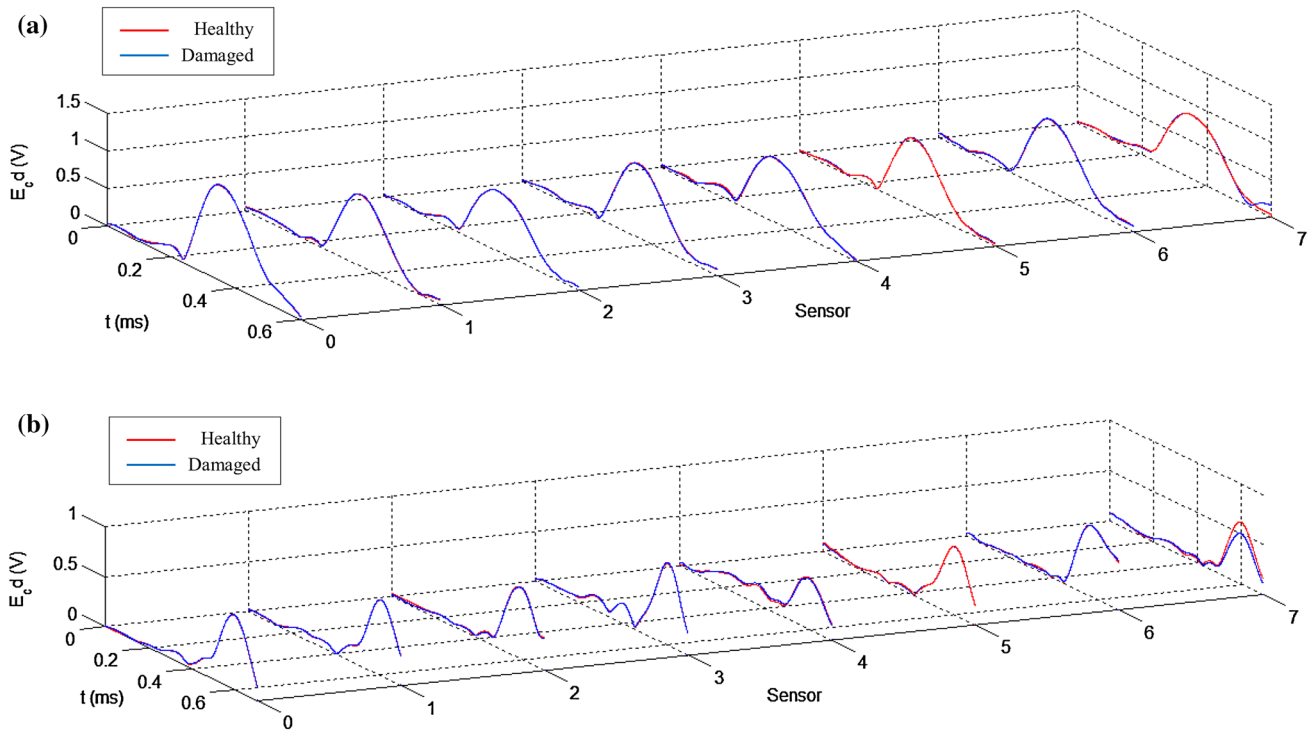
Fig. 14 Envelope of DWT coefficients of signals measured by sensors of: **a** internal and **b** external ring for damage at $R7_e$
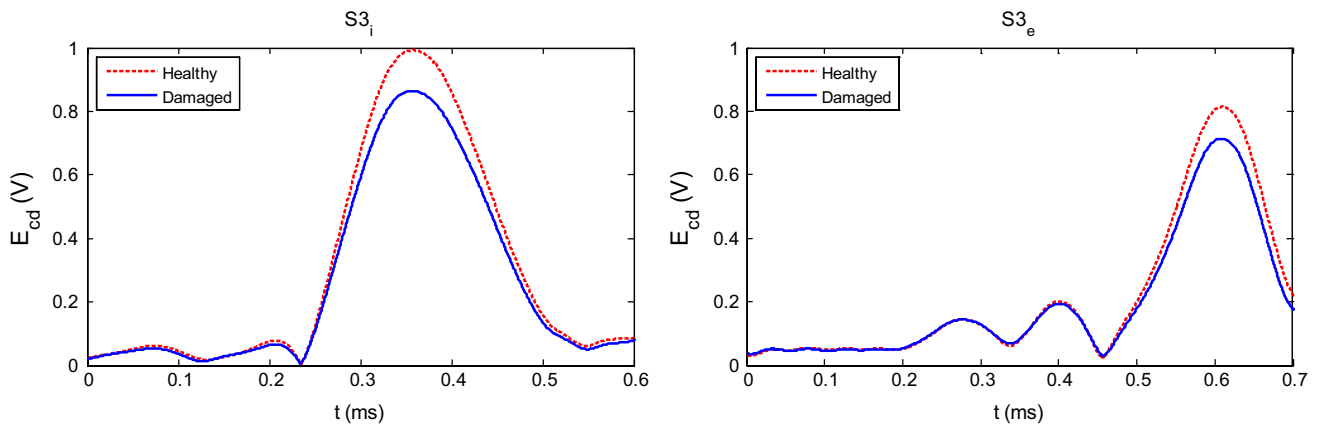

Fig. 15 Envelope of DWT coefficients of signals measured by sensors $S3_i$ and $S3_e$ for damage at $R3_i$

coefficients of signals measured by sensors of internal and external rings may be seen in Fig. 13.

The damage localized between actuator and $S0_i$ caused the amplitude decrease of the signal measured by this sensor. As internal and external sensors $S0_i$ and $S0_e$ are aligned, both signals presented an amplitude decrease. Therefore, it is possible to conclude as a rule that damage localized in one of the internal regions Rx_i causes an amplitude decrease of the signals measured by sensors of the internal and external rings.

Figure 14 shows the envelope of DWT coefficients of signals measured by sensors of internal and external rings with damage localized in the external region $R7_e$. In this case, only the signal amplitude measured by $S7_e$ significantly decreased, indicating damage in a region between this sensor and the actuator. In addition, internal ring sensors did not show significant difference. Based on these results, we conclude that a damage localized in external regions leads to an amplitude decrease of the signal measured by the external ring sensor while the signal measured by the internal
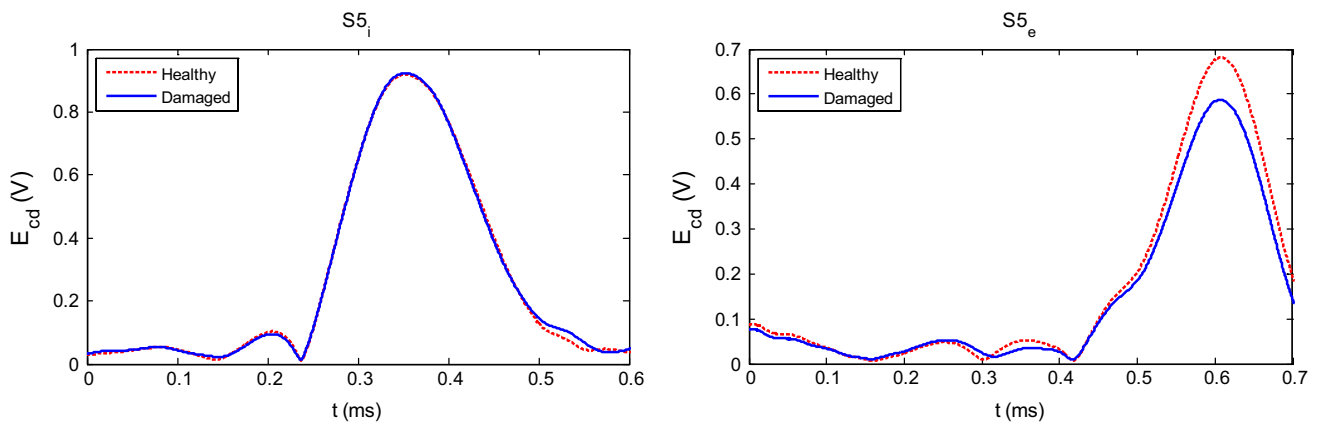
Fig. 16 Envelope of DWT coefficients of signals measured by sensors S5$_i$ and S5$_e$ for damage at R5$_e$
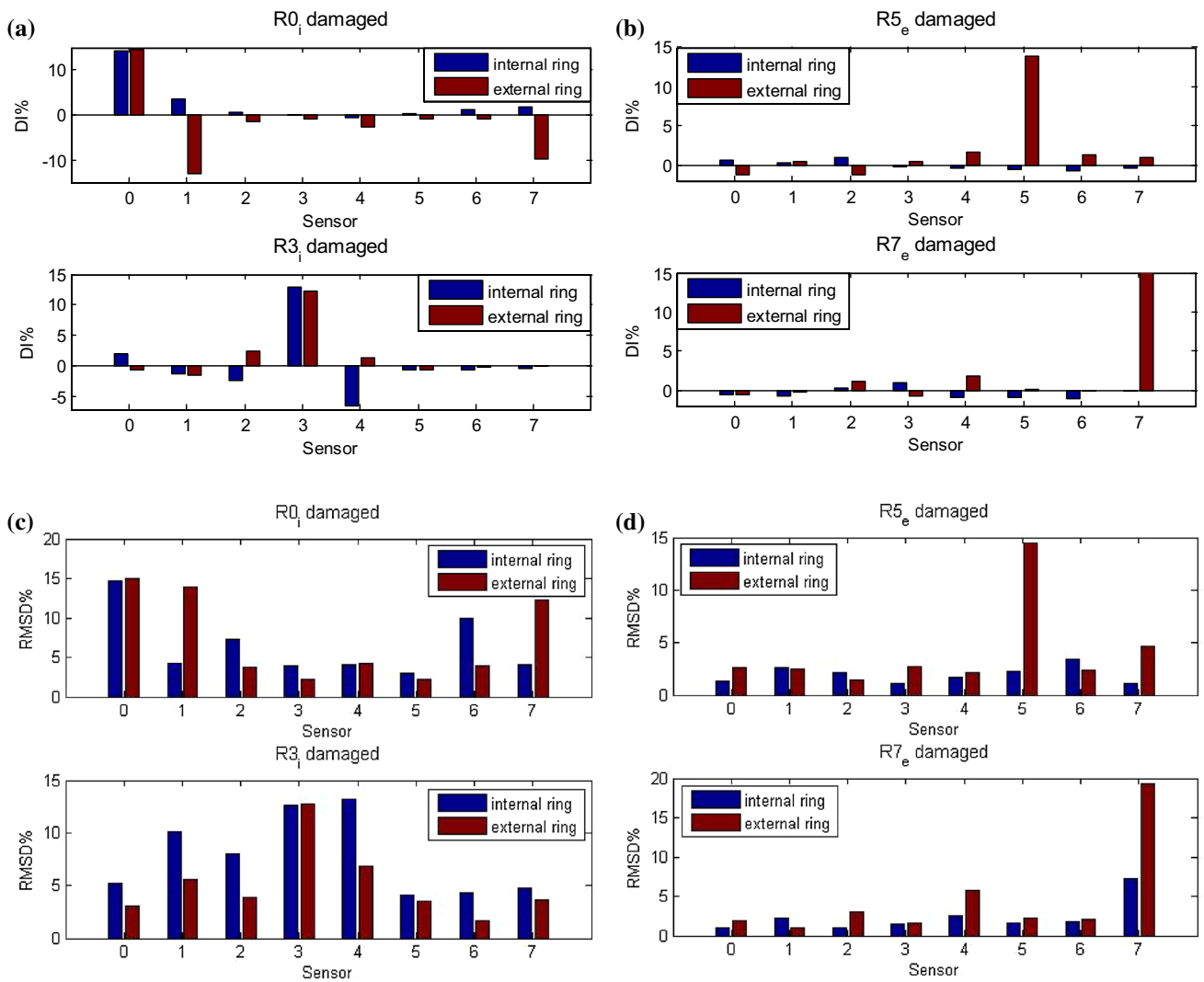

Fig. 17 Damage indices: **a**, **b** DI and **c**, **d** RMSD for regions R0$_i$, R3$_i$, R5$_e$ and R7$_e$ damaged
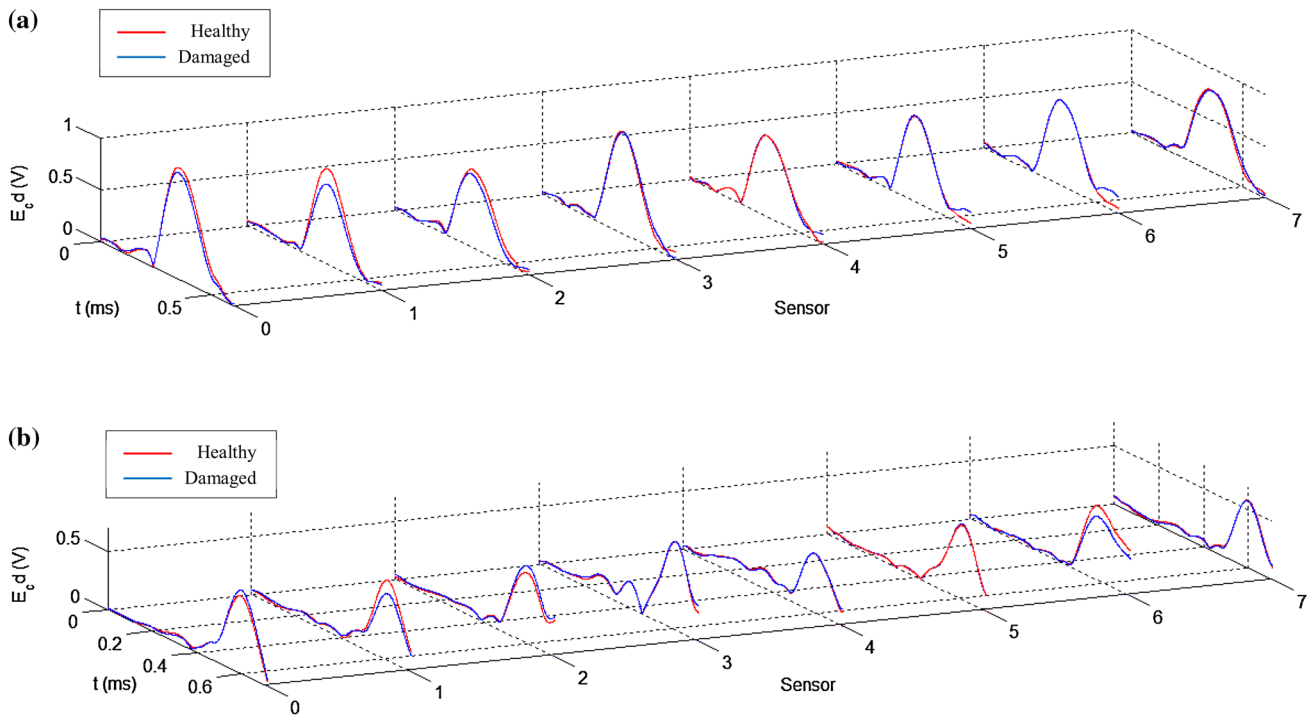
Fig. 18 Envelope of DWT coefficients of signals measured by sensors of: **a** internal and **b** external ring with regions R1$_i$ and R6$_e$ damaged

ring sensor is not significantly altered. Similar results were obtained in all the other experiments with this arrangement. Figures 15 and 16 shows the envelope of DWT coefficients of signals measured by sensors S3$_i$ and S3$_e$ for damage at R3$_i$ and S5$_i$ and S5$_e$ for damage at R5$_e$, respectively.

Analysis may be simplified using damage indices, shown in Fig. 17, where the results are subsumed. For R0$_i$ damage, S0$_i$ and S0$_e$ presented the highest DI of 14.1 and 14.5 %, respectively. Negative values of S1$_e$ and S7$_e$ are due to an increase in the signals amplitude measured by these sensors after R0$_i$ be damaged. This occurs due that part of the wave that propagates towards this region reflects in the damage and adds with the waves propagating between the actuator and the sensors S1$_e$ and S7$_e$. In the case of R3$_i$ damage, S3$_e$ and S3$_i$ also presented high DI corresponding to 12.9 and 12.3 %, respectively. On the other hand, for cases with R5$_e$ and R7$_e$ damage, only sensors of the external ring presented high DI, whereas in the first case, for the S5$_e$ was 13.9 %, and second, for the S7$_e$ was 18.5 %. Assessment of structure's integrity through RMSD was not conclusive. For example, S0$_e$, S1$_e$ and S7$_e$ presented high RMSD for damage localized at R0$_i$. As S1$_i$ and S7$_i$ presented low RMSD, the joint analysis of these indices shows that R1$_e$ and R7$_e$ are also damaged. The problem is that this index is sensitive to any change in signal format, while DI index indicates only changes in its amplitude. Furthermore, DI can differentiate when the signal amplitude raised or decreased by the signal of the index.

This configuration was also tested to detect and isolate more than a damaged region simultaneously. Figure 18 shows the envelope of DWT coefficients of signals measured by sensors of internal and external rings with the two masses positioned at R1$_i$ and R6$_e$. For the internal ring sensors, the signal amplitude measured by the S1$_i$ has been substantially decreased due to the presence of damage at R1$_i$. On the other hand, changes on signal measured by the sensor S6$_i$ were not significant, indicating that there is no damage at R6$_i$. For the external ring sensors, S1$_e$ and S6$_e$ presented a significant decrease in the amplitude of their signals. This occurred due to the presence of damage in these directions.

The DI and RMSD of each sensor of the arrangement for regions R1$_i$ and R6$_e$ damaged simultaneously are shown in Fig. 19. The high values of DI for sensors S1$_i$ (16.6 %) and S1$_e$ (16.8 %) indicate that the plate is damaged at region R1$_i$. Although the DI of S0$_i$ (4.68 %) and S2$_i$ (5.78 %) could point damages in these directions, this hypothesis is discarded by the negative values of the DI for S0$_e$ and S2$_e$ corresponding to the amplitude increase of the signals measured by these sensors. The high DI of S6$_e$ (14.4 %) indicates the presence of damage in this direction. Concurrently, the negligible DI of S6$_i$ (0.19 %) shows that the damaged region is the R6$_e$. The evaluation of the condition of structure through RMSD indices was not conclusive for this experiment. The values of RMSD for the sensors S1$_i$, S1$_e$, S2$_i$, S2$_e$, S6$_i$ and S6$_e$ were expressive. Using the

1362

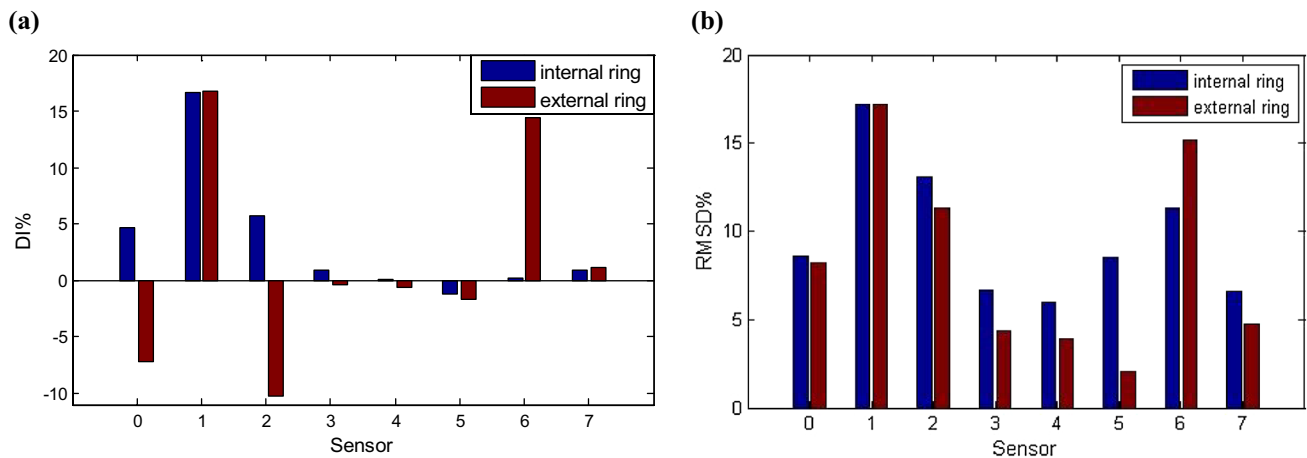J Braz. Soc. Mech. Sci. Eng. (2017) 39:1351–1363

(a)

(b)

Fig. 19 Damage indices: **a** DI and **b** RMSD with regions R1$_i$ and R6$_e$ damaged simultaneously

approach proposed in this paper, these indices erroneously indicate the presence of damage at R1$_i$, R2$_i$ and R6$_i$.

6 Conclusions

The development of strategies that use multisensor arrays on SHM systems play a crucial role to improve the efficiency on detect, locate and assess the onset of damages in structures. This paper presented a method for monitoring the integrity of structures, such as plates based on the propagation of Lamb waves and pitch–catch approach making use of multisensor arrays. The DWT and HT were used to process the measured signals to improve accuracy on evaluation of the first peak amplitude used to calculate the DI of the sensors arrangement. The expanded uncertainty of the measurement system was adopted to define the threshold between healthy and damaged structure, i.e., damage is detected when the signal measured by a sensor presents DI greater than its expanded uncertainty. The joint analysis of DI of the sensors arrangement promoted the detection, localization and assessment of damage severity inside the monitored area. The two ring-shaped arrangement of piezo transducers enabled a decrease in the region's extent monitored by each sensor. In this case, the monitored area was divided into sixteen regions. From the experimental results, we conclude that when an internal region is damaged, signals measured by sensors of internal and external rings of its direction result on a high and positive DI. On the other hand, for the case in which one of the external regions is damaged, only the sensor of external ring of its direction will result on a high and positive DI.

The analyzes using the RMSD index were not conclusive for the experiments made with the damage at boundary of two regions and using the two ring-shaped arrangement,

showing that this index is not suitable for the technique proposed in this paper.

Although the proposed method had been effective, for it to be applied to real structures, it is necessary to develop an embedded system to replace the bench lab equipment used in the experiments of this paper, capable to assess the structural integrity in real time. Another important aspect is the use of artificial intelligence techniques to generate the automatic diagnosis of the structure based on the proposed DI.

References

1. Wang X, Su Z (2009) Design of active sensor network and multilevel data fusion. Encyclopedia of structural health monitoring. Wiley, UK
2. Zhao X, Royer LR, Owens SE, Rose JL (2011) Ultrasonic Lamb wave tomography in structural health monitoring. Smart Mater Struct 20(10):1–10
3. Giridhara G, Rathod VT, Naik S, Mahapatra DR, Gopalakrishnan S (2010) Rapid localization of damage using a circular sensor array and Lamb wave based triangulation. Mech Syst Signal Process 24(8):2929–2946
4. Rathod VT, Mahapatra DR (2011) Ultrasonic Lamb wave based monitoring of corrosion type of damage in plate using a circular array of piezoelectric transducers. NDT&E Int 44(7):628–636
5. Su Z, Wang X, Chen Z, Ye L, Wang D (2006) A built-in active sensor network for health monitoring of composite structures. Smart Mater Struct 15(6):1939–1949
6. Malinowski P, Wandowski T, Ostachowicz W (2011) Damage detection potential of a triangular piezoelectric configuration. Mech Syst Signal Process 25(7):2722–2732
7. Alleyne DN, Cawley P (2016) PVDF multielement lamb wave sensor for structural health monitoring. IEEE Trans Ultrason Ferroelectr Freq Control 63(1):178–185
8. Lu Y, Wang X, Tang J, Ding Y (2008) Damage detection using piezoelectric transducers and the Lamb wave approach: II. Robust and quantitative decision making. Smart Mater Struct 17(2):1–13

9. Wang X, Lu Y, Tang J (2008) Damage detection using piezoelectric transducers and the Lamb wave approach: I. System analysis. Smart Mater Struct 17(2):1–15

10. Su Z, Ye L (2009) Identification of damage using lamb waves: from fundamentals to applications. Springer, Berlin

11. Lichtenwalner PF, Sofge DA (1998) Local area detection in composite structures using piezoelectric transducers. In: Proceedings SPIE symposium on smart structures and materials, San Diego, CA

12. Mallat SG (1989) A theory for multiresolution signal decomposition: the wavelet representation. IEEE Trans Pattern Anal Mach Intell 11(7):674–693

13. Colom-Palero RJ, Gadea-Girones R, Ballester-Merelo FJ, Martínez-Peiro M (2004) Flexible architecture for the implementation of the two-dimensional discrete wavelet transform (2D-DWT) oriented to FPGA devices. Microprocess Microsyst 28(9):509–518

14. Nibouche M, Nibouche O (2002) Design and implementation of a wavelet block for signal processing applications. In: 9th International conference on electronics, circuits and systems, Dubrovnik, Croatia

15. Chilo J, Lindblad T (2008) Hardware implementation of 1D wavelet transform on an FPGA for infrasound signal classification. IEEE Trans Nucl Sci 55(1):9–13

16. Feldman M (2011) Hilbert transform in vibration analysis. Mech Syst Signal Process 25(3):735–802

17. Pfeiffer H, Wevers M (2007) Pseudo-defects for the validation and tuning of structural health monitoring in plate-like structures using lamb waves, In: EU project meeting on aircraft integrated structural health assessment (AISHA), Leuven, Belgium

18. Kessler SS, Shim DJ (2005) Validation of a Lamb wave-based structural health monitoring system for aircraft applications. In: Proceedings of the SPIE's 12th international symposium on smart structures, San Diego, CA

19. Al-Adnani NNA, Mustapha F, Sapuan S, Saifulnaz MR (2016) Structural health monitoring and damage identification for composite panels using smart sensor. J Intell Mater Syst Struct. doi:10.1177/1045389X16629553

20. Zhu H, Luo H, Ai D, Wang C (2016) Mechanical impedance-based technique for steel structural corrosion damage detection. Measurement 88:353–359

21. ISO (1995) Guide to the expression of uncertainty in measurement. ISO, Geneva